

THE MOBILITY OF ZIRCONIUM AND IDENTIFICATION OF SECONDARY Zr-BEARING PHASES IN BAUXITE FROM POÇOS DE CALDAS, MINAS GERAIS, BRAZIL: A MASS-BALANCE AND X-RAY ABSORPTION SPECTROSCOPIC STUDY

LAURE DUVALLET[§]

*Laboratoire de Minéralogie-Cristallographie, UMR 5563 CNRS, Université Paul Sabatier,
39, Allées Jules-Guesde, F-31000 Toulouse, France et Instituto de Geociências, Universidade de São Paulo,
Rua do Lago 562, Cidade Universitaria, Caixa Postal 11348, Cep 05422-970, São Paulo, SP, Brasil*

FRANÇOIS MARTIN[§]

*Laboratoire de Minéralogie-Cristallographie, UMR 5563 CNRS, Université Paul Sabatier,
39, Allées Jules-Guesde, F-31000 Toulouse, France*

FRANÇOIS SOUBIÈS[§]

ORSTOM, UR12 Géosciences de l'Environnement Tropical, 32, Avenue Henri Varagnat, F-93143 Bondy, France

STEFANO SALVI

*Laboratoire de Minéralogie-Cristallographie, UMR 5563 CNRS, Université Paul Sabatier,
39, Allées Jules-Guesde, F-31000 Toulouse, France*

ADOLFO JOSE MELFI[§]

*Departamento de Geofísica, Instituto Astronômica e Geofísica, Universidade de São Paulo,
Caixa Postal 30627, Cep 01051, São Paulo, SP, Brasil*

JEAN-POL FORTUNÉ

*Laboratoire de Minéralogie-Cristallographie, UMR 5563 CNRS, Université Paul Sabatier,
39, Allées Jules-Guesde, F-31000 Toulouse, France*

ABSTRACT

The geochemistry and mineralogy of Zr have been studied in a bauxitic profile derived from a nepheline microsyenite at Poços de Caldas, Minas Gerais, southeastern Brazil. The Zr in the parent rock is hosted by the sorosilicate hainite (5–6% ZrO₂) and a Ca–Na amphibole (0.1–0.2% ZrO₂). Comparison of the variations in Zr, Ti, Nb and Th contents as function of the apparent density of different zones in the top few meters of the saprolite shows Th to be the least mobile element of the profile. Therefore, it was chosen as an invariant constituent in order to evaluate the mobility of other elements, especially the Zr. Mass-balance calculations demonstrate the leaching of Zr all along the profile, with a rate of removal of up to 40% at the weathering front. In the residual bauxitic materials, Zr is essentially localized in ferruginous products such as goethite-rich plasma filling the pores, and granules within the gibbsite-dominant matrix. Its mineralogical expression appears to be within polyhedra with an average of 6.6 O atoms, and average Zr–O distances of 2.16 Å, probably in adsorption on the surface of goethite in the pores and in granules of the gibbsite-rich matrix.

Keywords: bauxite, thorium, mass balance, zirconium, mobilization, X-ray absorption spectroscopy, baddeleyite, Poços de Caldas, Brazil.

SOMMAIRE

La géochimie et la minéralogie du zirconium ont été étudiées dans un profil latéritique provenant d'une syénite du complexe de Poços de Caldas, état du Minas Gerais, dans le sud-est du Brésil. La teneur en Zr de la roche mère provient de deux silicates:

[§] E-mail addresses: lorduval@usp.br, martin@ict.fr, soubies@orstom.rio.net, ajmelfi@usp.br

la hainite (5–6% ZrO₂) et une amphibole Ca–Na (0.1–0.2% ZrO₂). Des comparaisons effectuées sur les variations des teneurs en Ti, Nb et Th en fonction des densités apparentes des différentes zones sur les premiers mètres de la saprolite montrent que le thorium est l'élément le plus immobile du profil. La concentration en Th est invariante par rapport à celle des autres éléments et permet de calculer des balances de masse, spécialement pour Zr. Les observations montrent que le Zr est lessivé dans tous les horizons du profil, avec un taux de lixiviation de 40% en ZrO₂ au front d'altération. Dans la bauxite, le Zr se trouve dans des polyèdres de coordination ayant 6.6 atomes d'oxygène, en moyenne, avec une distance moyenne de 2.16 Å, probablement en adsorption à la surface des plasmas riches en goethite en cutanes dans les pores et dans les granules de la matrice riche en gibbsite.

Mots-clés: bauxite, thorium, mass balance, zirconium, mobilisation, spectroscopie d'absorption des rayons X, baddeleyite, Poços de Caldas, Brazil.

INTRODUCTION

Zirconium is commonly considered an immobile element during weathering processes. The accumulation of residual Zr in materials formed under supergene alteration has been widely documented over the years (*e.g.*, Goldschmidt 1937, 1954, Gordon & Murata 1952, Degenhardt 1957, Adams & Richardson 1960, Benelavskii 1963, Zeissink 1971, Erlank *et al.* 1978). As expected, the greatest concentrations reported are from strongly leached environments, such as in lateritic bauxites, where Zr can easily become concentrated by a factor of 3 to 4 (Adams & Richardson 1960).

The immobility of this element can be easily explained by (i) the fact that Zr generally occurs in the rocks as zircon, which is known to be a mineral highly resistant to dissolution (*e.g.*, Milnes & Fitzpatrick 1989), and (ii) the extremely low solubility of Zr in aqueous solutions (Levinson 1980, Brookins 1988). As a result, zirconium has often been used as an immobile element to evaluate mass transfer in weathered profiles (*e.g.*, Brimhall *et al.* 1991, Freyssinet 1994).

However, the high Zr content of many bauxites cannot be accounted for solely by the amount of zircon present. Degenhardt (1957), Benelavskii (1963) and Zakrutkin & Shvetsiva (1974) have suggested that Zr in bauxites can occur also as colloidal oxides or hydroxides (ZrO₂·*n*H₂O), more or less sorbed on secondary minerals, and can isomorphically replace iron and aluminum in the structure of oxyhydroxides or kaolinite. It has also been suggested that zircon stability may be lowered and Zr mobility enhanced in some strongly acid and organic-matter-rich media, such as podzols (Swindale & Jackson 1956, Ronov *et al.* 1961, Kimura & Swindale 1967, Berrow *et al.* 1978, Tejan Kella *et al.* 1991). A review of this subject can be found in Milnes & Fitzpatrick (1989). Lastly, Colin *et al.* (1993) and Braun *et al.* (1993) have questioned, with stronger arguments than Carroll (1953) produced in the past, the "axiomatic immobility" of zircon in soils and the use of zirconium as an invariable element in mass-balance calculations. This brief overview points to the likelihood that some mobilization of Zr and dissolution of zircon can occur in specific surficial environments. However, the neoformed secondary zirconiferous phases have not been well characterized yet.

This paper deals with a Brazilian occurrence of bauxite developed on nepheline microsyenite in the Poços de Caldas area, in the state of Minas Gerais. We here provide evidence for the mobilization of Zr during a lateritization process along a profile down to the bedrock, and thus confirm the inference of Soubières *et al.* (1991) on the basis of field observations. We bring new chemical, mass-balance and spectroscopic data to bear on the question of Zr mobilization. Furthermore, we report on the crystal chemistry of the secondary zirconiferous phases.

GEOLOGICAL SETTING

The Poços de Caldas complex is one of the largest alkaline bodies in the world, forming a large circular body of almost 800 km² (diameter 30–35 km, 1300 m altitude) at the boundary of the Minas Gerais and São Paulo states, southeastern Brasil (Fig. 1). Nepheline syenites or microsyenites (locally known as "tinguaite") and phonolites, along with ankaratritic lavas and pyroclastic rocks, are the main components of this Upper Cretaceous intrusion.

The aluminous syenitic rocks have been intensely transformed to bauxite as a consequence of the tropical climate. The Morro do Cristo deposit, where the profile PCMC-2 chosen for study is to be found, is located along the northern border of the complex. The very good drainage, the high and irregular relief (1500–1700 m altitude) and the steep slopes of this area have led to intense and rapid weathering of the parent rock (tinguaite), resulting in the formation of a bauxitic mantle in abrupt contact with the fresh rock (Fig. 2).

DESCRIPTION OF THE PROFILE

Parent rock

The tinguaite of Morro do Cristo, a dark grey and virtually aphanitic rock, consists of a mosaic of fine-grained nepheline and alkali feldspar in which small prisms of aegirine-augite (200 × 100 μm) are dispersed. Larger crystals (0.5–1 mm) of a complex fluorine-bearing Ti, Zr sorosilicate of Ca and Na identified as hainite (Atencio *et al.* 1999) and a Na–Ca amphibole (ferro-edenite) also are dispersed in the felsic groundmass. Hainite forms long

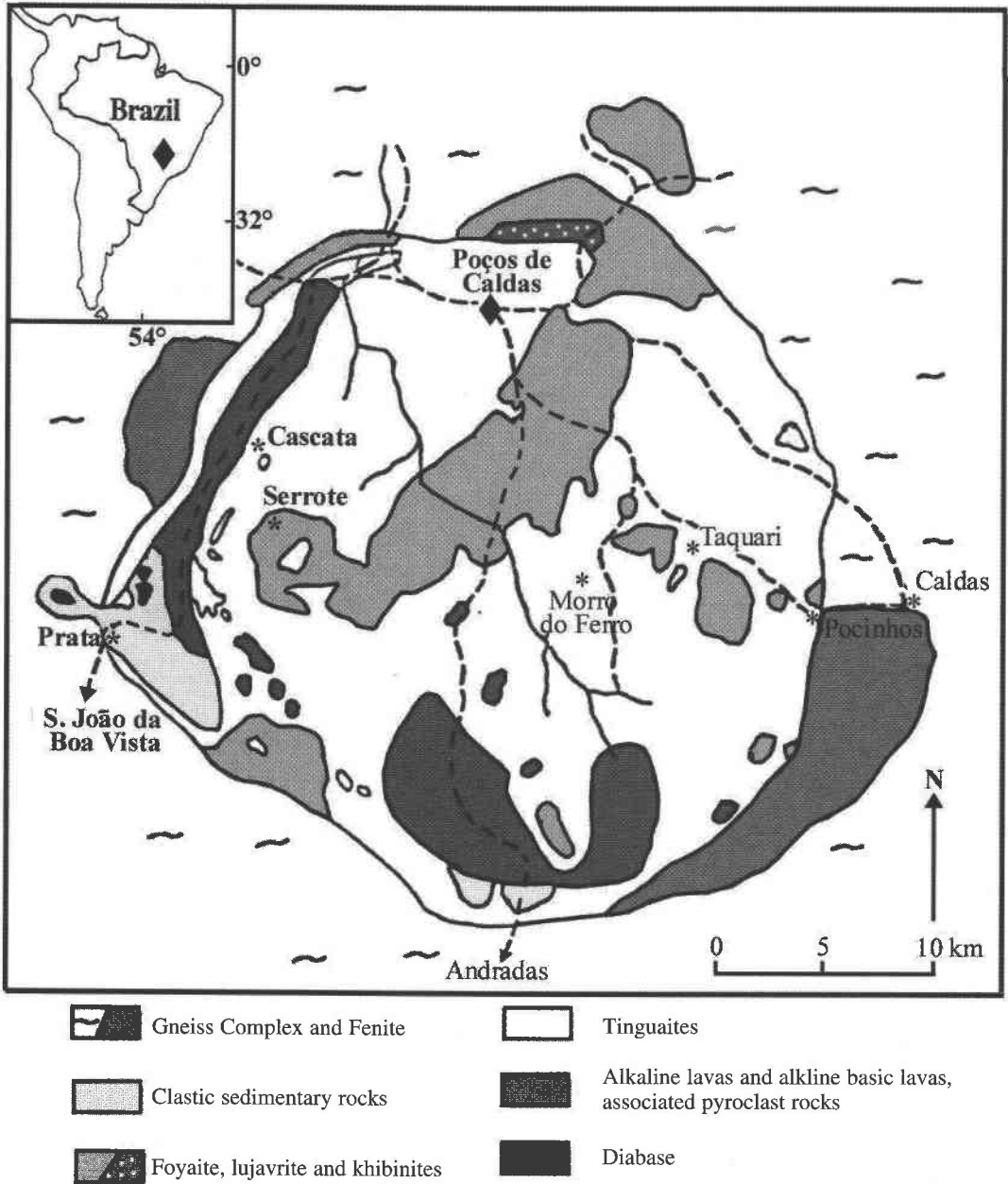


FIG. 1. General geology and location of the Poços de Caldas alkaline igneous complex (after Ellert 1959, Björnberg 1959). Diamond: study area.

poikilitic crystals, with high relief and birefringence to blue colors of the second order. Aegirine-augite comprises about 20% of the rock by volume, whereas other mafic minerals account for about 5%. Aegirine-augite is present in fine prisms of dark green color, and ferrodendrite forms larger, poikilitic crystals of dark brown

color. Zircon forms minute euhedral crystals, but is extremely rare. With an agpaitic index $[(Na + K)/Al]$ of about 1.2, and a high content of Zr, Nb and the rare-earth elements (*REE*) (Tables 1, 2), this nepheline microsyenite plots close to the limit between the agpaitic and miaskitic groups (*cf.* Sørensen 1974).

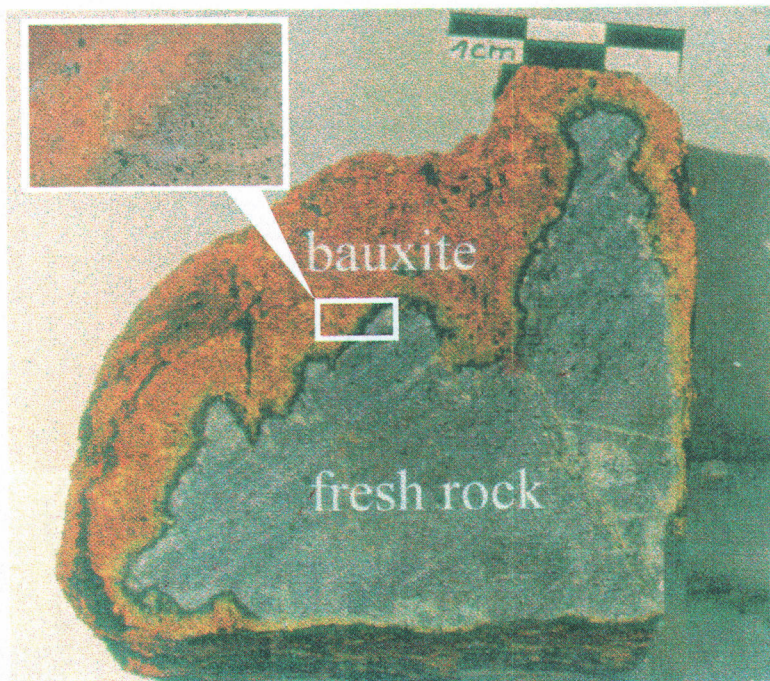


FIG. 2. Isovolumetric alteration at the contact with the microsyenite.

Electron-microprobe analyses (Soubières *et al.* 1991) have shown that hainite (their “giannettite”) is the principal Zr-bearing mineral in this rock (~5–6% ZrO₂). The electron-microprobe data gathered for hainite from Morro do Cristo fit well with the general structural formula $(A,B)_8(\text{Si}_2\text{O}_7)_2(\text{F})_4$, where *A* stands for Ca, Na, REE, and *B* stands for Ti, Zr, Mn, Fe, Nb, Ta, and Al, as given by Johan & Cech (1989). One of the best analyses gives the following empirical formula on the basis of 18 (O, F): $(\text{Na}_{0.947}\text{Ca}_{0.053})_{\Sigma 1} (\text{Ca}_{4.277}\text{Ce}_{0.069}\text{Sr}_{0.069}\text{Y}_{0.015})_{\Sigma 4.43} [(\text{Ti}_{0.896}\text{Zr}_{0.360}\text{Mn}_{0.186}\text{Nb}_{0.073}\text{Fe}_{0.049}\text{Al}_{0.001})_{\Sigma 1.565}\square_{0.436}] (\text{Si}_{3.900}\text{O}_{14.62}) \text{F}_{3.38}$. Zr also is present in the sodic-calcic amphibole (~0.1–0.2 % ZrO₂).

Numerous fine fissures cut the Morro do Cristo tinguaita in all directions. Locally, the tinguaita has been hydrothermally transformed over a few centimeters along the margins of the fissures to a light grey mixture of talc-like and unidentified interstratified clay minerals.

The PCMC-2 bauxitic profile

Five main horizons, each with transitional contacts, can be distinguished from bottom to top of this six-meter profile (*cf.* Soubières *et al.* 1991) (Fig. 3):

(a) Isalteritic bauxite (600–500 cm): Showing a sharp contact with the underlying fresh syenite, this

horizon consists of highly porous and friable reddish material, characterized by a very low density (1.1–1.4 g/cm³). It is cut by some vuggy veins, which arise from the transformation of the hydrothermally affected material.

(b) Nodular bauxite (500–350 cm): From bottom to top, this horizon illustrates the progressive destruction of the primary structures due to the formation of meganodules (Fig. 4). These consist of dm-banded reddish to yellowish spheroidal structures with a compact and harder cortex (density about 1.5–1.7 g/cm³), surrounded by a vuggy, highly porous material.

(c) Transitional level (350–230 cm): higher in the profile, a denser, more compact yellowish horizon gradually replaces the underlying spheres. Here the pore space is partly filled by a brownish clayey material illuviated from the upper horizons.

(d) Massive bauxite (230–190 cm): a level consisting of discontinuous, massive reddish to yellowish bauxite.

(e) Pebbly bauxite (190–0 cm): this reddish to yellowish nodular horizon occurs below a fine-textured organic soil (about 2 m thick). It consists mainly of fragments of the underlying horizon: small compact blocks (density about 1.9 g/cm³) are dispersed in a brown clayey matrix.

X-ray-diffraction analyses revealed that gibbsite (~75%) and goethite (~15%) are the major phases

TABLE 1. MAJOR-ELEMENT COMPOSITIONS OF SELECTED SAMPLES TAKEN FROM THE BAUXITIC PROFILE (PCMC-2), POÇOS DE CALDAS, MINAS GERAIS, BRAZIL

Horizon (*)	Depth (cm)	Sample class	SiO ₂	Al ₂ O ₃	Fe ₂ O ₃	MnO	MgO	CaO	Na ₂ O	K ₂ O	TiO ₂	P ₂ O ₅	H ₂ O*	H ₂ O*	Total
Pebbly bauxite (0-190 cm)	20	G (3)	0.34	57.89	7.11	0.02	<0.01	0.06	<0.01	<0.01	0.93	0.14	32.16	0.54	99.19
		m	4.65	48.15	7.60	0.05	<0.01	<0.01	<0.01	<0.01	1.29	0.14	33.56	2.59	98.03
	50	G (2)	0.34	58.73	6.43	0.05	<0.01	0.05	<0.01	<0.01	0.88	0.13	31.32	0.39	98.32
		m	3.24	51.50	8.52	0.06	0.02	<0.01	<0.01	<0.01	1.38	0.13	31.39	2.33	98.57
	100	G	0.38	58.62	7.50	0.03	<0.01	0.06	<0.01	<0.01	0.98	0.11	31.87	0.39	99.94
		m	2.24	52.33	10.09	0.07	<0.01	0.02	<0.01	<0.01	1.48	0.17	30.97	1.92	99.29
150	G	0.47	57.24	7.29	0.04	<0.01	<0.01	<0.01	<0.01	1.01	0.15	31.72	0.59	98.51	
	m	2.09	51.63	8.78	0.06	<0.01	<0.01	<0.01	<0.01	1.31	0.13	31.11	1.37	96.48	
Massive bauxite (190-230 cm)	210	(3)	0.27	57.29	7.85	0.04	<0.01	<0.01	0.02	0.03	1.12	0.13	31.60	0.42	98.77
Transitional level (230-350 cm)	300	N	0.27	57.72	8.45	0.05	<0.01	0.06	<0.01	0.01	1.19	0.08	31.16	0.50	99.49
Nodular bauxite (350-500 cm)	350	N	0.53	60.41	5.11	0.01	<0.01	<0.01	<0.01	<0.01	0.69	0.11	32.15	0.43	99.44
		M	1.14	44.65	19.95	0.54	<0.01	<0.01	<0.01	0.33	2.95	0.26	25.89	0.97	96.68
	400	M	2.26	53.25	11.55	0.14	<0.01	<0.01	<0.01	<0.01	1.68	0.24	29.03	0.97	99.12
		N (2)	0.47	58.54	6.49	0.04	<0.01	<0.01	<0.01	<0.01	0.91	0.16	31.97	0.25	98.84
Isalteritic bauxite (500-600 cm)	500	B	0.30	55.29	9.79	0.07	<0.01	<0.01	<0.01	<0.01	1.37	0.20	30.73	0.44	98.19
		V	0.35	55.92	9.45	0.04	<0.01	<0.01	<0.01	<0.01	1.24	0.20	30.77	0.45	98.42
	600	B ₁	0.35	56.56	9.79	0.16	<0.01	<0.01	<0.01	<0.01	1.37	0.25	30.64	0.56	99.68
		B ₂	1.19	55.84	9.70	0.07	<0.01	<0.01	<0.01	<0.01	1.33	0.22	30.46	0.67	99.48
	> 600	V	0.40	56.20	9.35	0.25	<0.01	0.03	<0.01	<0.01	1.24	0.23	30.91	0.43	99.04
		Fresh rock	> 600	55.83	20.90	3.94	0.25	0.21	1.45	7.67	7.54	0.51	0.18	0.97	0.04

Compositions are quoted in wt% oxide. Shown in parentheses in the column labeled "Sample class" is the number of samples analyzed (mean reported). * Pebbly bauxite: coarse gibbsite-rich gravels (G) with clayey matrix (m). Massive bauxite: more coherent horizon in which the underlying nodules are less sharply defined. Nodular bauxite: concentric spheres (N) (dm) with highly porous matrix (M); see Figure 4. Isalteritic bauxite: finely porous gibbsite-rich mass (B) cut by some fine (cm) and vuggy veins (V); B₁ and B₂ are two different samples collected at the contact of the fresh rock.

TABLE 2. TRACE-ELEMENT CONCENTRATIONS (ppm) IN SELECTED SAMPLES (§) TAKEN FROM THE BAUXITIC PROFILE (PCMC-2), POÇOS DE CALDAS, MINAS GERAIS, BRAZIL

Horizon	Depth (cm)	Sample class	Zr	Nb	Th	La	Ce	Nd	Sm	Eu	Dy	Er	Yb	Y	ΣLREE (*)	ΣHREE (**)
Pebbly bauxite (0 - 190 cm)	20	G (3)	735	518	67	2	389	2	4	0.4	<0.5	3	1	1	397	5
		m	575	629	91	8	686	6	2	0.4	<0.5	5	2	7	702	14
	50	G (2)	982	508	55	4	227	2	1	0.3	<0.5	3	1	1	234	5
		m	704	649	110	10	941	7	2	0.4	1	5	2	6	960	14
	100	G	618	552	69	10	351	4	2	0.2	3	3	1	1	367	8
		m	1003	702	109	11	876	8	4	0.3	1	5	2	6	899	13
150	G	649	594	76	8	534	5	1	0.3	114	3	1	3	548	121	
	m	979	686	110	10	969	8	13	0.3	1	5	2	7	1000	15	
Massive bauxite (190 - 230 cm)	210	(3)	1389	610	70	5	382	4	5	0.2	36	3	1	2	396	42
Transitional level (230 - 350 cm)	300	N	2502	643	85	5	492	4	2	0.3	1	4	1	2	503	8
Nodular bauxite (350 - 500 cm)	350	N	535	378	43	8	222	3	3	<0.1	1	3	1	1	236	6
		M	5778	1423	586	45	6962	32	10	2	5	12	7	20	7051	44
	400	M	3232	937	179	19	1866	9	3	1	3	7	3	10	1898	23
		N (2)	1222	534	48	5	48	2	1	0.2	<0.5	3	1	1	56	5
Isalteritic bauxite (500 - 600 cm)	500	M	2320	696	76	5	342	4	1	0.3	1	4	1	2	352	8
		B	2570	824	74	2	138	2	2	0.3	1	5	1	1	144	8
	600	V	2609	790	89	4	430	2	<0.5	0.4	<0.5	5	1	2	436	8
		B ₁	1583	841	82	3	146	3	3	0.3	<0.5	5	1	2	155	8
	> 600	B ₂	1292	815	74	3	163	4	3	0.3	<0.5	5	1	2	173	8
		V	1799	750	81	5	498	4	3	0.2	<0.5	5	1	2	510	8
Fresh rock	> 600		1057	296	36	234	344	109	18	4	9	7	4	42	709	62

(§) Data are reported here for the same samples as in Table 1.

(*) ΣLREE: Σ light rare-earth elements (La + Ce + Nd + Sm + Eu).

(**) ΣHREE: Σ heavy rare-earth elements (Dy + Er + Yb + Y).

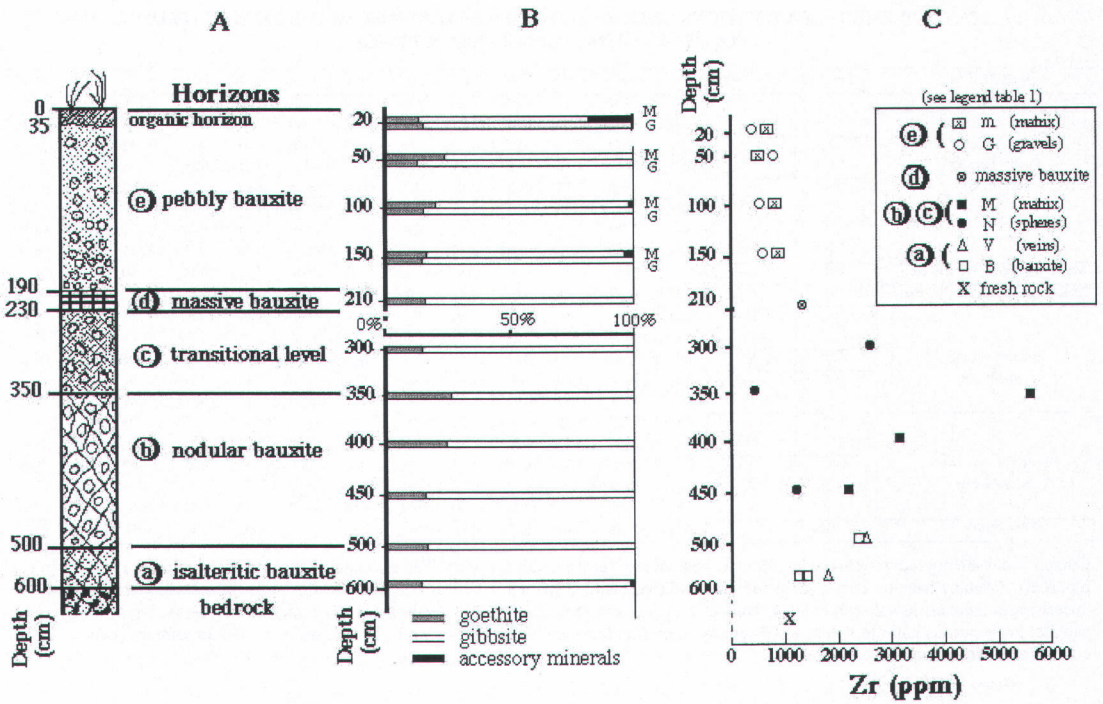


FIG. 3. Sketch of the profile studied (A), accompanied by mineralogical composition from XRD data (B) and Zr distribution (ICP-AES data) along it (C).

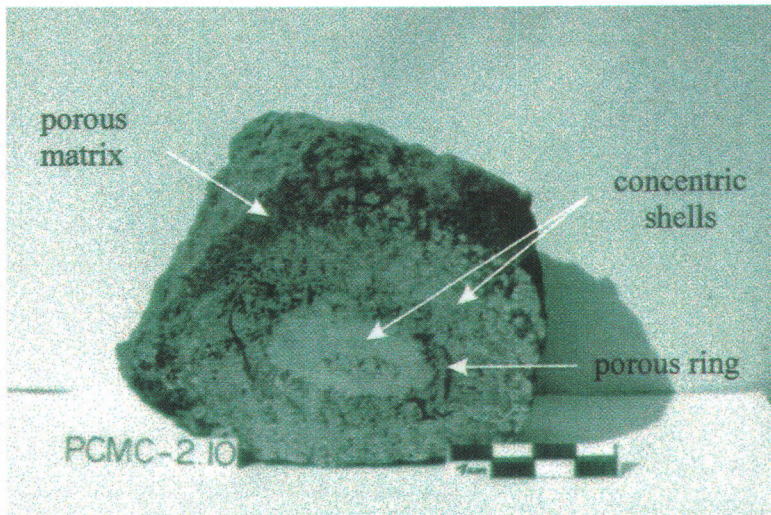


FIG. 4. Section of a nodule (400 cm depth) showing compact concentric shells (hard gibbsitic mass) separated by more porous rings and surrounded by a porous matrix.

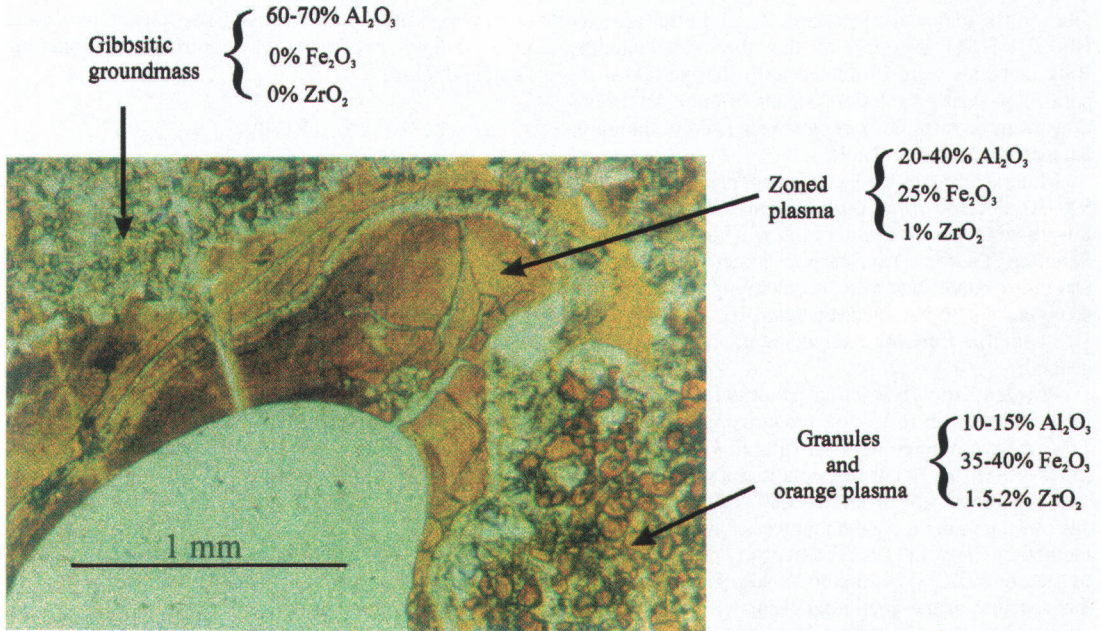


FIG. 5. Thin section of the bauxite (350 cm depth) in plane-polarized light. Scale bar is positioned over a pore space.

everywhere in the profile. Small amounts of kaolinite, anatase, rutile and quartz also were detected (accessory minerals, Fig. 3).

Microscopic observations

From bottom to top of the profile, the numerous thin sections that were examined show a very similar micro-organization for all the bauxitic materials. They reveal a mosaic of large crystals of gibbsite (10–30 μm) and numerous ferri-ferrous granules (a few to tens of mm) scattered in the compaction-induced voids (Fig. 5). These granules, more abundant in material from the vuggy veins, are orange-reddish in color, and have a strong relief and round to subhedral shapes. They are isotropic or very weakly birefringent, and commonly zoned and cracked.

The gibbsite-rich groundmass is criss-crossed by a system of large channels or interconnected vugs (ten of μm to mm in size) that are better developed in the friable horizons and vuggy veins than in the compact material. These voids are generally coated or infilled by two types of products, associated or not (Fig. 5): (i) a reddish brown, isotropic or slightly birefringent plasma, showing a low relief; these coatings are usually microlaminated (clayey illuvial deposits) and may represent fine gibbsite-dominant bands, and (ii) cracked irregular masses or bands of an orange ferri-ferrous plasma, optically homogeneous and with a high relief, very similar to the ferri-ferrous granules in the gibbsite-

rich groundmass. Orange plasma and granules do not appear to replace the phenocrysts, and are interpreted as weathering-induced neofomed products. Relics of hainite, amphibole and aegirine-augite are only observed in the first tens of cm of the saprolite. They have a very different appearance; they do not present any special form, and are dark brown in color.

ANALYTICAL PROCEDURES

In order to minimize the error in mass-balance calculations due to a possible heterogeneity in the distribution of trace-element-bearing minerals, we sampled relatively large amounts of all materials. The fresh tinguaitite, free of secondary iron oxyhydroxides, is believed to represent the parent rock for the entire PCMC-2 profile, and was used as the geochemical reference in this study. Owing to the very fine grain-size of this microsyenite and its homogeneity in thin sections, about 5 kg of fresh rock were collected from various parts of the outcrop. Any weathered part was carefully eliminated before preparing the samples for chemical analysis. As for the various bauxitic horizons, representative samples (1–2 kg) of each facies (matrix, nodules, veins) were collected and processed in a similar manner.

In preparation for analysis, samples were crushed, partitioned and pulverized ($\leq 250 \mu\text{m}$ particles). Chemical analyses of bulk samples were done by inductively coupled plasma – atomic emission spectroscopy (ICP-AES; Varian Liberty 200) after LiBO₂ fusion and HCl

dilution for major elements and Zr, and after a mixed HF-HCl-HNO₃ digestion for the other trace elements. Bulk densities were estimated with the method using paraffin as coating solution. Means of three determinations of three different samples were used in the mass-balance calculations (Table 3).

Mineral analyses were carried out using a CAMECA SX-50 electron microprobe fitted with three wavelength-dispersion spectrometers (Université Paul Sabatier, Toulouse) on carbon-coated thin sections. Operating conditions were: accelerating voltage 15 kV, beam current 10 nA, electron beam 10 μm across, with 10 s counting time for each element, and 5 s for background.

Powder X-ray-diffraction patterns for each sample were collected in reflection mode using a Philips PW 1130 diffractometer with Ni-filtered CuKα radiation (30 kV, 30 mA). Recording conditions were of 3.5 s by step of 0.0005° (2θ) from 2° to 80° (2θ). The percentage of each mineral constituent was evaluated using the method of Rietveld (1969) from X-ray powder data (4 s by step of 0.02°). This method also permitted to refine the structure of the goethite present.

⁵⁷Fe Mössbauer absorption spectra (Laboratoire de Chimie de Coordination, Toulouse) were recorded over the range ±14 mm/s in 512 channels to characterize the Fe-bearing phases. The Mössbauer spectrometer is composed of a compact γ-detector system for high count-rates and a conventional constant-acceleration Mössbauer Wisel device. A ⁵⁷Co (in Rh) source with nominal activity of 50 mCi was used. Spectra were collected at temperatures of 298 and 70 K, and recorded on a Canberra multichannel analyzer, linked to a computer. The isomer shift was recorded with respect to α-Fe metal. The absorbing sample was prepared with less than 10 mg Fe/cm², to avoid the effect of absorber thickness. Lorentzian line-shapes were assumed for deconvolution, using least-square fitting procedures. The χ² and misfit values were calculated in order to evaluate the goodness of the computer fit. For this analysis, samples were finely ground in acetone (to minimize possible oxidation of Fe).

To obtain some information on the crystallographic site of Zr in the ferri-ferrous phases of the bauxite, we ran a number of absorption spectra at the LURE synchrotron facility (Orsay, France), on the D44 station. The DCI storage ring was operated at 1.85 GeV and 246 mA. A Si (311) double crystal was used to monochromatize the X-ray beam. EXAFS (X-ray absorption fine structure) spectra at the Zr K edge were collected in transmission mode at room temperature with energy steps of 2 eV over the energy range 17.9–18.9 keV, and with an acquisition time of 2 seconds per step. XANES spectra at the Zr K edge were collected with energy steps of 1 eV over the energy range 17.95–18.1 keV, and with an acquisition time of 1 second by step. Spectra were calibrated by reference to metallic Zr (Zr K edge at 17998 eV). Samples were finely ground, and the resulting pow-

ders were sandwiched between two pieces of kapton tape. Sample absorbance was controlled by adjusting sample thickness.

RESULTS

Mass-balance calculations

Two independent methods are generally used to estimate element mobility during weathering processes: the "isovolume" and the "isoelement" methods (Braun *et al.* 1993). In the first case, if the volume of a horizon can be considered unaffected by the weathering processes, relative gains and losses in the concentration of any element, compared with its concentration in the parent rock, are given by: % change = $[(x \cdot \rho / x_0 \cdot \rho_0) - 1] * 100$, where x and x_0 are the element concentrations, and ρ and ρ_0 the bulk densities, of the weathered material and of the parent rock, respectively (Millot & Bonifas 1955).

If, on the other hand, evidence exists that the concentration of any given element did not change, *i.e.*, the element was immobile during weathering, the percentage increase or decrease of any other element in the weathered rock relative to the fresh rock can be calculated (Nesbitt 1979): % change = $[(x/i) / (x_0/i_0)] - 1 * 100$, where x and x_0 refer to the same parameters as above, and i and i_0 are the concentrations of the immobile element in the weathered and in the fresh rock, respectively. Cramer & Nesbitt (1983) pointed out that owing to uncertainties in sample representativity, density measurements and results of chemical analyses, only changes in concentration greater than ±20% can be considered significant in these calculations.

In the present study, both methods of calculation were used to monitor chemical changes in the PCMC-2 profile, with the particular objective to characterize the behavior of Zr during bauxite formation. The concentrations of the major and selected trace elements used for these calculations are reported in Tables 1 and 2.

The isovolume method (Table 3) was only applied to the lowermost meter of the bauxite (isalteritic horizon, Fig. 3), where large- and small-scale structural and textural features (*e.g.*, mineral distribution and shape, organization of fractures) of the parent rock are very well preserved (Fig. 2). With these calculations, we looked for an immobile element that could be used with the isoelement method to estimate Zr mobility during the first stage of weathering, as well as in those parts of the profile where textural evidence for volume conservation were not found. Data for vuggy veins of the isalteritic bauxite were not taken into consideration because their parent rock (hydrothermally transformed tinguaitite) was not analyzed, and because they represent only a small percentage of the profile.

Focusing on Zr, Ti, Nb and Th, commonly considered as immobile in secondary environments, Table 3 shows that: i) Zr experiences a surprisingly large

TABLE 3. ISOVOLUMETRIC MASS-BALANCE: LOSSES (-) AND GAINS (+) (%) IN COMPARISON WITH THE FRESH ROCK AT THE BASE OF THE PCMC-2 PROFILE

Horizon	Depth (cm)	Sample class	Si	Al	Fe	Mn	Mg	Ca	Na	K	Ti	P	Zr	Nb	Th	Σ LRREE (*)	Σ HREE (**)	D
Isalteritic bauxite (500 - 600 cm)	500	B	-100	19	11	-87	-100	-100	-100	-100	20	-50	9	25	-8	-91	-94	1.17
	600	B1	-100	10	1	-74	-100	-100	-100	-100	9	-44	-39	15	-7	-91	-95	1.06
		B2	-99	23	13	-87	-100	-100	-100	-100	20	-44	-44	27	-5	-89	-94	1.20

Same samples as in the table 1

D: density (g/cm^3) of the materials. D = 2.62 g/cm^3 for the fresh rock.

TABLE 4. ISOTHORIUM MASS-BALANCE: LOSSES (-) AND GAINS (+) (%) IN COMPARISON WITH THE FRESH ROCK AT THE BASE OF THE PCMC-2 PROFILE

Horizon	Depth (cm)	Sample class	Si	Al	Fe	Mn	Mg	Ca	Na	K	Ti	P	Zr	Nb	Σ LRREE (*)	Σ HREE (**)
Isalteritic bauxite (500 - 600 cm)	500	B	-100	29	21	-86	-100	-100	-100	-100	31	-46	18	35	-90	-94
	600	B1	-100	19	9	-72	-100	-100	-100	-100	18	-39	-34	25	-90	-94
		B2	-99	30	20	-86	-100	-100	-100	-100	27	-41	-41	34	-88	-94

Data are reported here for the same samples as in Table 1.

(*) Σ LRREE: Σ light rare-earth elements (La + Ce + Nd + Sm + Eu).

(**) Σ HREE: Σ heavy rare-earth elements (Dy + Er + Yb + Y).

decrease at the contact with the fresh rock; ii) as expected, Ti and Nb accumulate in the weathered material with respect to the fresh rock; iii) Th seems to be the least mobile element in the saprolite, as already noted by Braun *et al.* (1993) in similar environments. Obviously, these results are only valid insofar as the distribution of these elements was homogeneous in the parent rock. Our observations indicate that this is the case for the fresh tinguaita sampled within a few hundred meters of the profile.

Using Th as an invariable element, we can apply the second method of mass-balance calculation to the whole profile, in particular, to the upper parts, where the original structure and texture of the tinguaita are least preserved (Tables 4, 5). Considering the structural heterogeneity of the upper levels and the limited number of analyses done, only the most obvious trends in Tables 3 to 5 will be considered.

Si, Na, Ca, K and Mg

As is always observed in cases of strong ferrallitic weathering, these elements are almost entirely leached in the first centimeters away from the fresh rock.

Zr

In the lower part of the profile (below 500 cm), both methods of mass-balance calculation showed a 30–40% loss in Zr (Tables 3, 4). Therefore, there is a little doubt

that at Morro do Cristo, an important proportion (up to 40%) of the Zr content of the parent rock is leached during the early stages of weathering. Zr leaching is still more effective in the upper (and older) parts of the profile (above 190 cm), with Zr losses up to 70–80% from the massive bauxite to the surface. A loss also is evident in the uppermost part of the nodular bauxitic horizon (400–350 cm). Sandwiched between these three levels of high degree of Zr leaching, two levels of weaker Zr mobilization occur (Table 5). These can be explained as 1) levels of absolute accumulation, whereby Zr was supplied by the leaching of the overlying horizons, 2) the expression of some degree of parent-rock heterogeneity or, alternatively 3) the consequence of a change that could have occurred in the drainage conditions of the area represented by the PCMC-2 profile.

The mobility of Zr in the Morro do Cristo profile is among the highest ever reported in the literature. This high degree of mobility could be related to the fact that the principal Zr-bearing primary mineral is not zircon but the Na–Ca silicate hainite, in which Zr is octahedrally coordinated and, as a result, more easily removed than in the zircon structure. Furthermore, there is an abundance of fluorine in this mineral (~7–8%), fluorine being known to be a very efficient ligand for Zr in solution. Nevertheless, we have still no clear evidence that Zr is transported in a dissolved form in the area studied; a colloidal form, which could be a suspension of zirconiferous particles neoformed in the bauxite (see below), should be also considered.

TABLE 5. ISOTHORIUM MASS-BALANCE (%) ALONG THE ENTIRE PCMC-2 PROFILE, POÇOS DE CALDAS, MINAS GERAIS, BRAZIL

Horizon	Depth (cm)	Sample class	Si	Ti	Al	Fe	Mn	Mg	Ca	Na	K	Tl	P	Zr	Nb	ΣLREE (*)	ΣHREE (**)
Pebbly bauxite (0 - 190 cm)	20	G (3)	-100	-2	49	-3	-96	-100	-97	-100	-100	-2	-58	-63	-6	-70	-96
		m	-100	0	-9	-24	-92	-100	-100	-100	-100	0	-69	-78	-16	-61	-91
	50	G (2)	-100	13	84	7	-87	-100	-98	-100	-100	13	-53	-39	12	-78	-95
		m	-98	-11	-19	-29	-92	-100	-100	-100	-100	-11	-76	-78	-28	-56	-93
	100	G	-100	0	46	-1	-94	-100	-98	-100	-100	0	-68	-69	-3	-73	-93
		m	-100	-4	-17	-15	-91	-100	-99	-100	-100	-4	-69	-69	-22	-58	-93
	150	G	-100	-6	30	-12	-92	-100	-100	-100	-100	-6	-60	-71	-5	-63	-8
		m	-99	-16	-19	-27	-92	-100	-100	-100	-100	-16	-76	-70	-24	-54	-92
Massive bauxite (190 - 230 cm)	210	(3)	-100	13	41	2	-92	-100	-99	-100	-100	13	-63	-32	6	-71	-57
Transitional level (230 - 350 cm)	300	N	-100	-17	16	-9	-91	-100	-98	-100	-100	-1	-81	0	-8	-70	-95
Nodular bauxite (350 - 500 cm)	350	N	-99	13	142	9	-97	-100	-100	-100	-100	13	-49	-58	7	-72	-92
		M	-100	-64	-87	-69	-87	-100	-100	-100	-100	-64	-91	-66	-70	-39	-96
	400	M	-99	-34	-49	-41	-89	-100	-100	-100	-100	-34	-73	-38	-36	-46	-92
		N (2)	-99	34	110	23	-88	-100	-100	-100	-100	34	-33	-13	35	-94	-94
	M	-100	0	30	-4	-90	-100	-100	-100	-100	0	-42	4	11	-76	-94	
Isalteritic bauxite (500 - 600 cm)	500	B	-100	31	29	21	-86	-100	-100	-100	-100	31	-46	18	35	-90	-94
		B ₁	-100	18	19	9	-72	-100	-100	-100	-100	18	-39	-34	25	-90	-94
	B ₂	-99	27	30	20	-86	-100	-100	-100	-100	27	-40	-40	34	-88	-94	

Data are reported here for the same samples as in Table 1.

(*) ΣLREE: Σ light rare-earth elements (La + Ce + Nd + Sm + Eu).

(**) ΣHREE: Σ heavy rare-earth elements (Dy + Er + Yb + Y).

Ti, Nb, Fe

These elements can broadly be considered as more or less immobile along the profile (weak leaching or absolute accumulation). An exception is the highly porous matrix material found in the intermediate part of the nodular bauxitic horizon (400–350 cm), where these elements are strongly leached, along with Zr and Al (see below). It is likely that part of the leached elements are trapped in the nodules, for which calculations invariably show a gain in mass.

Al

Al seems to be more mobile than Fe, Ti, and Nb, at least in the median and upper horizons, where elevated absolute accumulations occur in some gibbsite-rich nodular blocks (balance up to +100 %) and where matrices are systematically depleted in this element.

The rare earths

The rare earths are strongly leached along the whole profile, in particular the heavy rare earths. This process of leaching and fractionation is by and large similar to that observed by Braun *et al.* (1993) in their study of a lateritic profile derived from a syenite in Cameroon, and will not be discussed further in this paper.

Mineralogy of the bauxite

The bauxite of Morro do Cristo appears to be essentially composed of gibbsite and goethite (Fig. 3). Anatase, kaolinite, quartz and rutile were found as accessory minerals in some horizons.

Zr distribution in the bauxite

In order to assess the distribution of Zr in the bauxite, in the absence of a macroscopic Zr-bearing phase (Fig. 3), electron-microprobe analyses were performed on secondary phases and relics in each horizon of the profile. The analyses revealed the presence of 1–2% Zr in pore-filling products and in the surrounding orange granules. The orange plasma, the most ferrous of these pore-filling products, can contain up to 8% ZrO₂. All analyses of these ferrous products yielded low totals (about 70%), indicating that the material is highly porous or hydrated (or both). Results of semiquantitative electron-microprobe analyses show that Zr is well correlated with Fe and Ti (Fig. 6), suggesting that Zr is associated with one or both of these elements. A similar correlation was found in chemical analyses of bulk samples of bauxite, with correlation coefficients of 0.917 with Fe and 0.899 with Ti (Soubières *et al.* 1991). As Fe is a major component of these materials and the only one of the two elements to be present along the

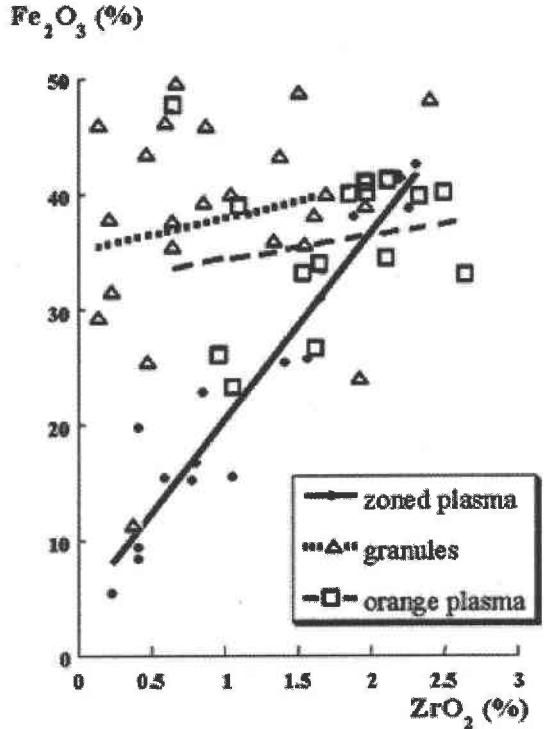


FIG. 6. Zr-Fe correlation, microprobe data.

whole profile (Fig. 3), we focussed on goethite, the only Fe-bearing phase found in the profile.

INVESTIGATIONS OF THE CRYSTAL CHEMISTRY OF Zr IN THE SECONDARY PHASES

Mössbauer spectroscopy of goethite

Goethite is a magnetically ordered mineral. The differences in Mössbauer spectra of natural samples of goethite depend on their chemical composition and the dimensions of the crystalline domains (Johnston & Norrish 1981). Ferruginous material from each bauxitic horizon of the Morro do Cristo profile has been analyzed by Mössbauer spectroscopy. The resulting spectra show a superparamagnetic couple at 298 K, and a sextuplet at 70 K with field value of 44 T and broadened lines. These data indicate that the Fe in the goethite is commonly substituted by a diamagnetic element. Al is the most likely candidate, as it commonly substitutes for Fe in goethite (Schulze 1984). Therefore, the variation of the cell parameters determined by Rietveld refinement of X-ray diffractograms collected from the same materials allowed us to calculate the extent of ^{IV}Al-for-Fe substitution on the basis of Schwertmann's

model (1984). About 30 mole % of the component AlOOH has been found in all samples of goethite; this value had been confirmed by Mössbauer spectroscopy analyses (Stucki 1985). Nevertheless, since Zr also is a diamagnetic element, it too could be incorporated in the structure, as suggested by Soubières *et al.* (1991), because the difference in ionic radius between Fe^{3+} and both Al and Zr in octahedral coordination is similar. To shed some light on the crystal chemistry of Zr in these materials, an X-ray absorption spectroscopy study was carried out.

XAFS spectroscopy on Zr K-edge

Some ferriferous pore-filling material taken from the bauxite of Morro do Cristo (PCMC-2) was analyzed by XAFS transmission spectroscopy.

Model compounds for XAFS data collection

Zr-bearing compounds having well-refined structures were chosen as models of characteristic environments for Zr in minerals. Nonmetamict zircon, ZrSiO_4 , is a model for a ^{81}Zr environment; ^{71}Zr environments occur in baddeleyite, ZrO_2 , zirkelite, $(\text{Ca,Th})\text{ZrTi}_2\text{O}_7$, and in aqueous complexes of Zr. Zr in sixfold coordination is most common in Zr-bearing alkali silicates such as catapleiite, $\text{Na}_2\text{ZrSi}_3\text{O}_9 \cdot 3\text{H}_2\text{O}$. All these references spectra were provided courtesy of François Farges. The baddeleyite used in the present study is synthetic reagent-grade monoclinic zirconia, 99% pure (Farges *et al.* 1994). The zircon used is synthetic also, but its spectrum is like that of natural non-metamict zircon (Farges & Calas 1990). The zirkelite comes from Sri Lanka; it was originally metamict, but was recrystallized by heating (Farges *et al.* 1993).

RESULTS

Zr X-ray absorption spectroscopy near-edge structure (XANES)

Zr K-edge XANES spectra (Fig. 7) for the selected model compounds and PCMC-2 show slight but significant differences, depending on the coordination environment of Zr. For the PCMC-2 spectrum, the absorption edge is in the same location and quite similar to the one of baddeleyite and zirkelite, which corresponds to a ^{71}Zr coordination. The similarities in the XANES spectra of PCMC-2, baddeleyite, and zirkelite also suggest that the individual Zr-O distances are similar.

Zr X-ray absorption spectroscopy fine structure (XAFS)

All XAFS spectra have been fitted between 0.9 and 10 \AA^{-1} since spectrum PCMC-2 is too noisy over this

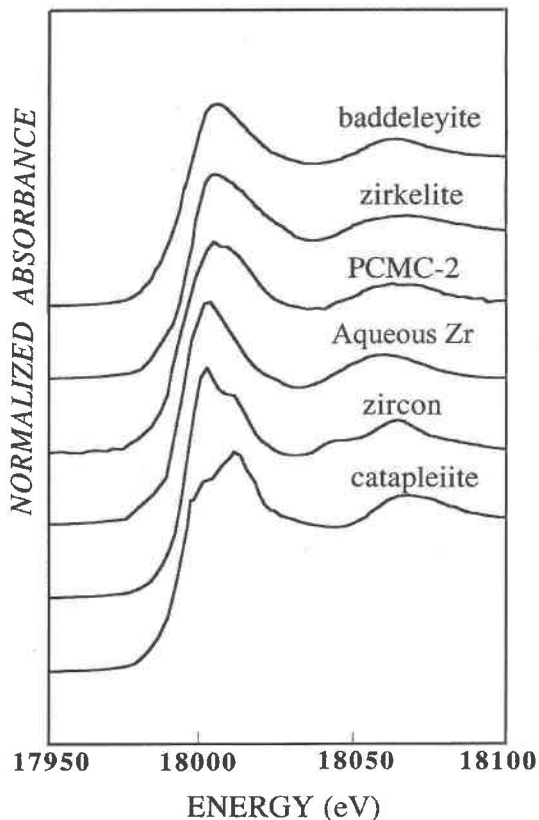


FIG. 7. Normalized XANES spectra on Zr K-threshold of Morro do Cristo sample (PCMC-2), and Zr-containing reference compounds (baddeleyite, catapleiite, zirkelite, zircon, aqueous Zr).

range. XAFS spectra for PCMC-2, baddeleyite and zirkelite are presented in Figure 8. Fourier transforms (FT) of the k^3 -weighted XAFS spectrum at the Zr K-edge (Fig. 9) for the reference compounds zircon, baddeleyite, aqueous Zr, catapleiite, and zirkelite are in good agreement with previous crystal-structure refinements (Farges & Calas 1991, Farges *et al.* 1993, 1994). The spectra depend essentially on the coordination number, but some disorder interaction in the structure may exist. Two groups of FT are distinguished depending on the intensity of their first peak. One group of FT is composed of zircon, catapleiite and aqueous Zr because of their high coordination number, or the high degree of crystallinity. The first peak of the FT of the zircon spectrum corresponds to ^{81}Zr , four O atoms at 2.13 Å and four others at 2.27 Å. The first peak of the FT of the aqueous Zr spectrum corresponds to ^{71}Zr , which is very well organized at short-range order, and the first peak of the FT of the catapleiite spectrum corresponds to ^{61}Zr in which the ZrO_6 polyhedra are regular (all Zr-O dis-

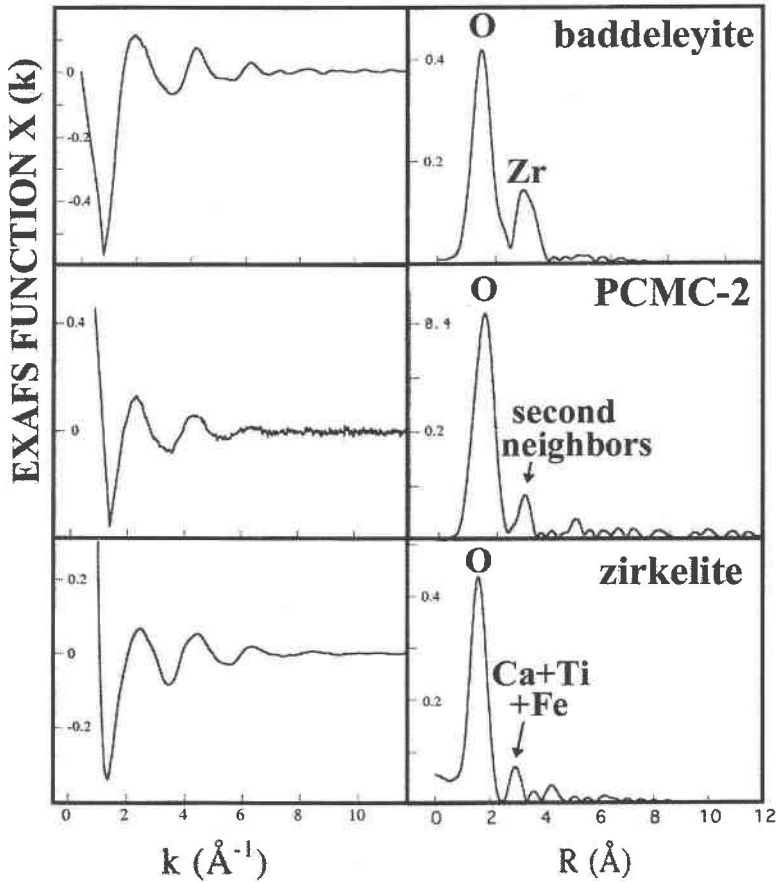


FIG. 8. Fourier transforms (FT) of the k^3 -weighted XAFS spectra at the Zr K-edge for PCMC-2, zirkelite and baddeleyite. Peaks on the Zr-X pair correlation functions are labeled to identify X.

tances are equal). The other group of FT is composed of baddeleyite (a seven-coordinated Zr mineral with weak organization at short range) and zirkelite, in which the first peak corresponds to seven atoms of oxygen.

The FT of PCMC-2 is in good agreement with the second group of FT, containing baddeleyite and zirkelite. The first peak for these two compounds corresponds to the first shell of Zr neighbors, which are seven atoms of oxygen (Figs 8, 9). The second peak corresponds to the second shell of neighbors. For baddeleyite, it corresponds to only Zr, and for zirkelite, to Ca, Ti and Fe neighbors.

O neighbors

The extracted edge-energy (E_0) values for PCMC-2, baddeleyite, and zirkelite are in good agreement with the one measured in catapleite. The low absolute value

for ΔE_0 ($|\Delta E_0| < 1.6$ eV) suggests that the empirical amplitude and phase-shift functions extracted from catapleite should provide a good calibration of the XAFS structural parameters. Because of its very well-determined structure, we used catapleite as reference to fit XAFS spectra. Zr in catapleite is known to be in a regular polyhedron of six O atoms at 2.073 Å.

Inverse Fourier transforms and least-squares fits of the O first-neighbor contribution to the Zr XAFS of the baddeleyite with two sheets show that the first peak in the FT corresponds to Zr-O correlations of an average of 7.3 O atoms at an average distance of 2.17 Å (Farges & Calas 1991, Farges *et al.* 1993, 1994). This result is in excellent agreement with structure-refinement data (Smith & Newkirk 1965) and previous XANES data.

Inverse Fourier transforms and least-squares fits of the O first-neighbor contribution to the Zr XAFS of PCMC-2 with two sheets show that the first peak in the

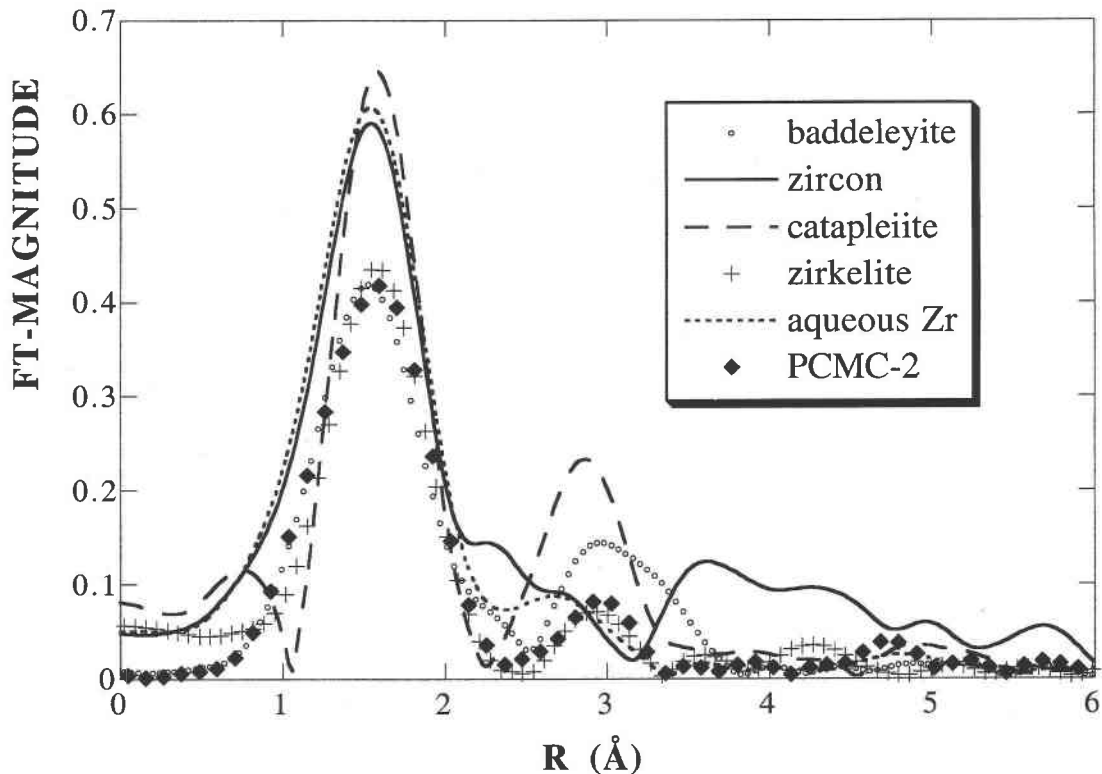


FIG. 9. Superposition of the Fourier transforms (FT) of the k^3 -weighted XAFS spectra at the Zr K-edge for PCMC-2, and reference compounds.

FT corresponds to Zr–O correlations of an average of 6.6 O atoms at an average distance of 2.16 Å (Debye–Waller-type factor $\Delta\sigma^2 = 2.8 \times 10^{-3} \text{ \AA}^2$). This result, in excellent agreement with previous XANES results, is quite similar to that of baddeleyite. Zr in PCMC-2 seems to have an atomic environment similar to that for baddeleyite.

Second neighbors

The second shell of coordination in baddeleyite is composed of seven atoms of Zr centered at 3.47 Å, whereas in zirkelite, it consists of one Ca atom at 3.24 Å, three Ti atoms at 3.25, 3.30 and 3.35 Å, two Fe atoms at 3.40 and 3.47 Å, one Ti atom at 3.53 Å, and three Ca atoms at 3.67 Å. Least-squares fit of the FT XAFS spectrum of baddeleyite and zirkelite are presented Figure 10. It seems that where the second neighbor is Zr (as in baddeleyite), the FT of the XAFS signal of its contribution shows a maximum around 5 \AA^{-1} ; where the second neighbor of Zr is “light” (as in zirkelite), the maximum of the FT is near the lower $k(\text{Å}^{-1})$ range.

The FT of PCMC-2 shows a second-neighbor contribution at an unrefined distance of 2.95 Å, but because of the low signal-to-noise ratio, information about the middle distance (10 to 15 Å^{-1}) is lost, and so is impossible to analyze quantitatively. However, qualitative analysis of the inverse FT for this RDF (radial distribution function) feature suggests the presence of a “light element”, as in the case for zirkelite. The PCMC-2 sample being essentially composed of Fe (goethite), we can suppose that the zirconium’s second-neighbor is Fe. The distance Zr–Fe of 2.95 Å must be corrected by phase pair (Zr–Fe) factor $\Phi_{\text{Zr-Fe}}$. But we already can estimate $\Phi_{\text{Zr-Fe}} = 2.3 \text{ \AA}$, and the distance Zr–Fe would be about 3.3 Å ($\pm 0.1 \text{ \AA}$). With the distances Zr–O (2.16 Å) and the distance $^{56}\text{Fe}^{3+}$ –O in goethite (2.04 Å), we calculated the value of the angle Zr–O–Fe to be about 105° . This value is typical of shared edges.

Our XANES and XAFS results show that Zr is located in sevenfold-coordinated sites in the ferrous phase of pore-filling in bauxite (PCMC-2) from Poços de Caldas. This result leads us to discard the hypothesis of Zr incorporation in the goethite structure, where it would be in the sixfold-coordinated site of Fe. Zr–O

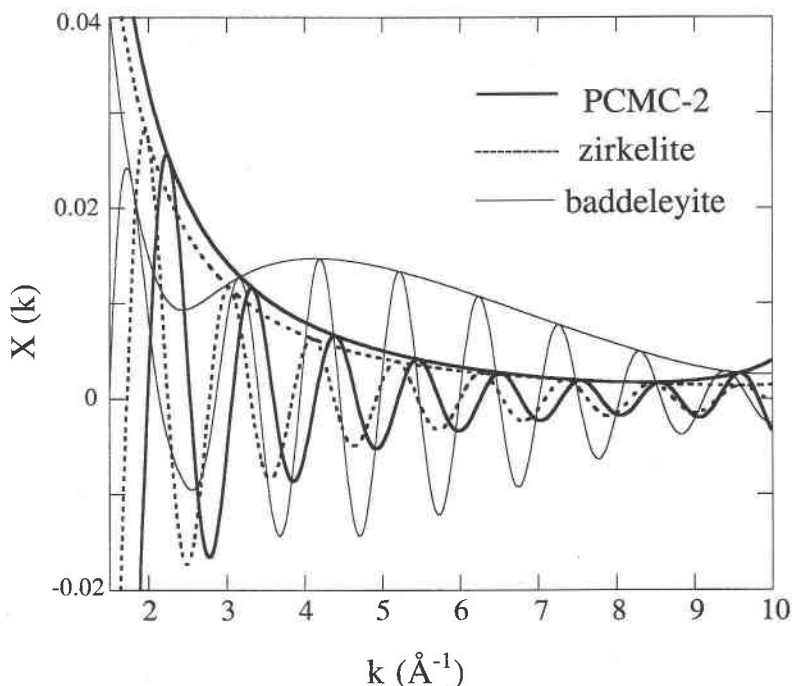


FIG. 10. Superposition of least-squares fit of the Fourier-filtered XAFS spectrum of baddeleyite, zirkelite and PCMC-2 sample at the Zr K edge. The fit for these compounds includes contributions from O nearest neighbors and second neighbors.

distances of 2.16 Å are similar to those in baddeleyite, but the second neighbors are probably Fe atoms, with Zr-Fe distances estimated at 3.3 Å. If the Fe is from goethite, it is possible to calculate the angle Zr-O-Fe to be about 105°, which is typical of an environment of edge-sharing. These results suggest that Zr is present in the goethitic plasma, and is located within a polyhedron of seven O atoms (with Zr-O distances about 2.16 Å) edge-sharing with Fe-bearing octahedra of the goethite.

CONCLUSIONS

In the Poços de Caldas area, Minas Gerais, Brazil, a profile across a thick section of bauxite developed on a nepheline microsyenite was examined in detail in order to investigate the behavior of Zr during supergene weathering. Field and microscopic observations suggest that this element was mobile. Evidence includes the total disappearance, during the first stages of weathering, of the primary Zr-bearing minerals (hainite and amphibole), and the occurrence of Zr in neoformed ferruginous products (goethite-rich plasma and granules) that do not replace primary minerals. In addition, mass-balance calculations demonstrate that Zr was leached from all horizons of the profile. The extent of leaching was calculated to reach 40% ZrO₂ at the weathering front.

A crystal-chemical study of the Zr-bearing ferruginous material revealed that Zr does not substitute for Fe in the goethite (the only ubiquitous Fe-bearing phase), as proposed by Soubières *et al.* (1991), but rather that it is present within polyhedra of 6.6 O atoms on average, with average Zr-O distances of 2.16 Å. This baddeleyite-like first shell of neighbors probably shares edges with Fe³⁺-bearing octahedra. This arrangement implies a radical change in the structure of the Zr-bearing phase, which in turn is yet another line of evidence that this cation was transported during the weathering process. Some improvements are needed to identify this Zr-bearing phase produced by the supergene weathering of hainite, and more geochemical data are needed to understand the role of F released from the hainite in the transport of Zr.

ACKNOWLEDGEMENTS

The staff of LURE is acknowledged for its assistance in the XAS measurements. We also thank Philippe Ildefonse for his XAS assistance, and Philippe de Parseval for his electron-microprobe analyses. References were graciously provided by F. Farges. We thank sincerely F. Farges for his help, his constructive review and many discussions. We also are grateful to J.

Delvigne and R.F. Martin for their constructive comments. Field work and analytical costs were underwritten by a grant from FAPESP.

REFERENCES

- ADAMS, J.A.S. & RICHARDSON, F.A. (1960): Thorium, uranium and zirconium concentration in bauxite. *Econ. Geol.* **55**, 1653-1675.
- ATENCIO, D., COUTINHO, J.M.V., ULBRICH, M.N.C., VLACH, S.R.F., RASTSVETAeva, R.K. & PUSHCHAROVSKY, D.YU. (1999): Hainite from Poços de Caldas, Minas Gerais, Brazil. *Can. Mineral.* **37**, 91-98.
- BENELAVSKII, S.I. (1963): *The Mineralogy of Bauxites*. Gosgeol. Tekhizdat, Moscow, Russia (in Russ.).
- BERROW, M.L., WILSON, M.J. & REAVES, G.A. (1978): Origin of extractable titanium and vanadium in the A horizon of Scottish podzols. *Geoderma* **21**, 89-103.
- BJÖRNBERG, A.J.S. (1959): Rochas clásticas do planalto de Poços de Caldas. *Bol. Fac. Filos. Ciências Letras Univ. São Paulo* **237**, *Geologia* **18**, 64-123.
- BRAUN, J.J., PAGEL, M., HERBILLON, A. & ROSIN, C. (1993): Mobilization and redistribution of REEs and thorium in a syenitic lateritic profile: a mass balance study. *Geochim. Cosmochim. Acta* **57**, 4419-4434.
- BRIMHALL, G.H., LEWIS, C.J., FORD, C., BRATT, J., TAYLOR, G. & WARIN, O. (1991): Quantitative geochemical approach to pedogenesis: importance of parent material reduction, volumetric expansion, and eolian influx in lateritization. *Geoderma* **51**, 51-91.
- BROOKINS, D.G. (1988): *Eh-pH Diagrams for Geochemistry*. Springer-Verlag, New York, N.Y.
- CARROLL, D. (1953): Weatherability of zircon. *J. Sed. Petrol.* **23**, 106-116.
- COLIN, F., ALARÇON, C. & VIELLARD, P. (1993): Zircon: an immobile index in soils? *Chem. Geol.* **107**, 273-276.
- CRAMER, J.J. & NESBITT, H.W. (1983): Mass balance relations and trace element mobility during continental weathering of various igneous rocks. *Sci. Géol. (Strasbourg), Mém.* **73**, 63-73.
- DEGENHARDT, H. (1957): Untersuchungen zur geochemischen Verteilung des Zirkoniums in der Lithosphäre. *Geochim. Cosmochim. Acta* **11**, 279-309.
- ELLERT, R. (1959): Contribuição à geologia do maciço alcalino de Poços de Caldas. *Bol. Fac. Filos. Ciências Letras Univ. São Paulo* **237**, *Geologia* **18**, 5-63.
- ERLANK, A.J., SMITH, H.S., MARCHANT, J.W., CARDOSO, M.P. & AHRENS, L.H. (1978): Zirconium. In *Handbook of Geochemistry*, vol. II-4, sect. 40 (K.H. Wedepohl, ed.). Springer-Verlag, Berlin, Germany.
- FARGES, F., BROWN, G.E., JR. & VELDE, D. (1994): Structural environment of Zr in two inosilicates from Cameroon: mineralogical and geochemical implications. *Am. Mineral.* **79**, 838-847.
- _____ & CALAS, G. (1991): Structural analysis of radiation damage in zircon and thorite: an X-ray absorption study. *Am. Mineral.* **76**, 60-73.
- _____, EWING, R.C. & BROWN, G.E., JR. (1993): The structure of metamict, aperiodic $(Ca,Th)_2Zr_2Ti_2O_{14}$. *J. Mater. Res.* **8**, 1983-1995.
- FREYSSINET, P. (1994): Gold mass balance in lateritic profiles from savanna and rain forest zones. *Catena* **21**, 159-172.
- GOLDSCHMIDT, V.M. (1937): The principles of the distribution of chemical elements in minerals and rocks. *J. Chem. Soc. London* **1**, 655-673.
- _____ (1954): *Geochemistry*. Clarendon Press, Oxford, U.K.
- GORDON, M., JR. & MURATA, K.J. (1952): Minor elements in Arkansas bauxite. *Econ. Geol.* **47**, 169-179.
- JOHAN, Z. & ČECH, F. (1989): Nouvelles données sur la hainite, $[Na_2Ca_4(Ti,Zr,Mn,Fe,Nb,Ta)_{1,50}\square_{0,50}](Si_2O_7)_2F_4$ et ses relations cristallographiques avec la götzenite, $Na_2Ca_5Ti(Si_2O_7)_2F_4$. *C.R. Acad. Sci. Paris* **308**, sér. II, 1237-1242.
- JOHNSTON, J.H. & NORRISH, K. (1981): A ^{57}Fe Mössbauer spectroscopic study of a selection of Australian and other goethites. *Aust. J. Soil Res.* **19**, 231-237.
- KIMURA, H.S. & SWINDALE, L.D. (1967): A discriminant function using zirconium and nickel for parent rocks of strongly weathered Hawaiian soils. *Soil Science* **104**, 69-76.
- LEVINSON, A.A. (1980): *Introduction to Exploration Geochemistry* (second ed.). Applied Publ. Ltd., Calgary, Alberta.
- MILLOT, G. & BONIFAS, M. (1955): Transformations isovolumétriques dans les phénomènes de latéritisation et bauxitisation. *Bull. Serv. Carte Géol. Alsace-Lorraine* **8**, 3-20.
- MILNES, A.R. & FITZPATRICK, R.W. (1989): Titanium and zirconium minerals. In *Minerals in Soils Environments* (J.B. Dixon & S.B. Weed, eds.; second edition), Soil Sci. Am., Madison, Wisconsin (1131-1205).
- NESBITT, H.W. (1979): Mobility and fractionation of rare-earth elements during weathering of a grandiorite. *Nature* **279**, 206-210.
- RIETVELD, H.M. (1969): A profile refinement method for nuclear and magnetic structures. *J. Appl. Crystallogr.* **2**, 65-71.
- RONOV, A.B., VAINSHTEIN, E.E. & TUZOVA, A.M. (1961): Geochemistry of hafnium, zirconium and some other hydrolyzate elements in clays. *Geochemistry* **4**, 343-355.

- SCHULZE, D.G. (1984): The influence of aluminium on iron oxides. VIII. Unit-cell dimensions of Al-substituted goethite and estimation of Al from them. *Clays Clay Minerals* **32**, 36-44.
- SCHWERTZMANN, U. (1984): The influence of aluminium on iron oxides. IX. Dissolution of Al-goethites in 6M HCl. *Clay Mineral.* **19**, 9-19.
- SMITH, D.K. & NEWKIRK, H.W. (1965): The crystal structure of baddeleyite (monoclinic ZrO₂) and its relations to the polymorphism of ZrO₂. *Acta Crystallogr.* **18**, 983-991.
- SØRENSEN, H. (1974): *The Alkaline Rocks*. John Wiley & Sons, New York, N.Y.
- SOUBIÈS, F., MELFI, A.J., DELVIGNE, J. & SARDELA, I.A. (1991): Mobilidade do zircônio na bauxitização de rochas alcalinas do maciço de Poços de Caldas, Minas Gerais. *Revista Brasileira de Geociências* **21**(1), 17-22.
- STUCKI, J.W. (1985): Iron in soils and clay minerals. *NATO Adv. Study Inst., Ser.* **217**. Reidel, Dordrecht, The Netherlands.
- SWINDALE, L.D. & JACKSON, M.L. (1956): Genetic processes in some residual podzolised soils of New Zealand. *Trans. Sixth Int. Congress Soil Science (Paris)* **37**, 233-239.
- TEJAN-KELLA, M.S. FITZPATRICK, R.W. & CHITTLEBOROUGH, D.J. (1991): Scanning electron microscope study of zircons and rutiles from podzol chronosequence at Cooloola, Queensland, Australia. *Catena* **18**, 11-30.
- ZAKRUTKIN, V.E. & SHVETSIVA, I.V. (1974): Zircon in the bauxites of the southern Timan region. *Litologiya i Polznye Iskopaemye* **5**, 32-40.
- ZEISSINK, H.E. (1971): Trace element behaviour in two nickeliferous lateritic profiles. *Chem. Geol.* **7**, 25-36.

Received July 29, 1998, revised manuscript accepted March 15, 1999.